https://doi.org/10.5194/essd-2020-99
Preprint. Discussion started: 15 June 2020

High-resolution mapping of circum-Antarctic landfast sea ice distribution, 2000-2018

Alexander D. Fraser[1,2,3], Robert A. Massom[4,2], Kay I. Ohshima[3], Sascha Willmes[5], Peter J. Kappes[6], Jessica Cartwright[7,8,2], and Rick Porter-Smith[2]

[1]Institute for Marine and Antarctic Studies, Hobart, Tasmania, Australia
[2]Antarctic Climate & Ecosystems Cooperative Research Centre, Hobart, Tasmania, Australia
[3]Institute of Low Temperature Science, Hokkaido University, Sapporo, Hokkaido, Japan
[4]Australian Antarctic Division, Kingston, Tasmania, Australia
[5]University of Trier, Germany
[6]Oregon Cooperative Fish and Wildlife Research Unit, Department of Fisheries and Wildlife, Oregon State University, USA
[7]National Oceanography Centre, Southampton, UK
[8]University of Southampton, Southampton, UK

Correspondence: Alexander Fraser (Alexander.Fraser@utas.edu.au)

Abstract. Landfast sea ice (fast ice) is an important component of the Antarctic nearshore marine environment, where it strongly modulates ice sheet-ocean-atmosphere interactions and biological and biogeochemical processes, forms a key habitat, and affects logistical operations. Given the wide-ranging importance of Antarctic fast ice and its sensitivity to climate change, improved knowledge of its distribution (and change and variability therein) is a high priority. Antarctic fast-ice mapping to date has been limited to regional studies and a time series covering East Antarctica from 2000 to 2008. Here, we present the first continuous, high spatiotemporal resolution (1 km, 15 day) time series of circum-Antarctic fast ice extent; this covers the period March 2000 to March 2018, with future updates planned. This dataset was derived by compositing cloud-free satellite visible-thermal infrared imagery using an existing methodology, modified to enhance automation and reduce subjectivity in defining the fast ice edge. This ground-breaking new dataset (Fraser et al., 2020) has wide applicability, and is available at http://dx.doi.org/doi:10.26179/5d267d1ceb60c. The new algorithm presented here will enable continuous large-scale fast ice mapping and monitoring into the future.

1 Introduction

Landfast sea ice (fast ice) is a pre-eminent feature of the Antarctic near-coastal environment, where it forms a relatively narrow (several tens to 200 kms wide) zone of consolidated ice attached to grounded icebergs, coastal margins (including sheltered embayments), floating glacier tongues and ice shelf fronts (World Meteorological Organization, 1970). Depending on location, it can be either annual (forming each austral autumn-winter and melting back each spring-summer) or perennial (Fraser et al.,

https://doi.org/10.5194/essd-2020-99
Preprint. Discussion started: 15 June 2020

2012), with multi-year fast ice attaining thicknesses up to several tens of metres (e.g., Massom et al., 2010). By forming a recurrent, persistent and highly-consolidated substrate of sea ice and snow, fast ice strongly modulates important physical and biological processes occurring at the Antarctic coastal margin - including stabilisation of ice shelves that moderate ice sheet mass loss to the ocean and resultant sea level rise (Massom et al., 2018). Given these factors, there is strong motivation for improved knowledge of its circum-Antarctic distribution, change and variability. Indeed, the lack of such information has been highlighted as a major gap by the Intergovernmental Panel on Climate Change (IPCC) Fifth Assessment Report (Vaughan et al., 2013) and the Special Report on Oceans and the Cryosphere (Meredith et al., 2019).

The consistent large-scale and long-term monitoring of Antarctic fast ice from space necessitates overcoming a number of inherent challenges relating to detection and resolution (both spatial and temporal), given the attributes of the satellite data themselves, and the nature of fast ice itself. For one thing, fast ice is a narrow remote-sensing target compared to the more extensive moving pack-ice zone (that is regularly monitored by coarse-resolution satellite passive-microwave sensors), and advection of pack ice against adjacent fast ice can lead to a relatively indistinct boundary between the two. Table 1 summarises the current status of Antarctic fast ice detection and mapping from space, and the advantages and disadvantages of the techniques used (see also Lubin and Massom, 2006). Wide-swath moderate-resolution satellite visible and thermal infrared (TIR) imagery offers excellent geographical coverage at kilometre-scale resolution and on daily time-scales, but it is strongly affected by persistent cloud cover year-round and polar darkness (the latter precluding use of visible imagery in winter) (Fraser et al., 2009). While this limitation can theoretically be circumvented by using high-resolution Synthetic Aperture Radar (SAR) imagery (Giles et al., 2008; Li et al., 2018; Kim et al., 2020), the application of SAR to large-scale fast-ice mapping and time-series analysis has to date been limited in space and time by its relatively-narrow swath coverage and uneven image acquisition around coastal Antarctica. Satellite passive-microwave data, on the other hand, offer complete circumpolar coverage on a daily basis (largely unaffected by clouds and darkness), but at a poorer spatial resolution of $\sim$6.25 km (Nihashi and Ohshima, 2015) to limit its capability for accurate fine-scale mapping of fast ice.

As a result of these challenges and factors relating to scientific focus, the mapping of Antarctic fast ice from space has to date been largely confined to limited geographical regions (e.g., around Antarctic bases and penguin colonies) and also relatively short time series or snapshots. These are based on manual interpretation of ad hoc digitizations of satellite SAR and cloud-free visible/TIR imagery (e.g., Mae et al., 1987; Ushio, 2006; Massom et al., 2009; Aoki, 2017; Kim et al., 2018; Li et al., 2018; Giles et al., 2008; Labrousse et al., 2019; Kim et al., 2020). A significant advance in continuous coverage was made by Fraser et al. (2012) in their analysis of fast ice across East Antarctica (10° W to 172° E) based on compositing of cloud-free imagery from the MODerate-resolution Imaging Spectro-radiometer (MODIS) sensors onboard Aqua and Terra, for the period 2000-2008. This study also used a more rigorous definition of fast ice that included a temporal criterion e.g., that sea ice must remain stationary for 20 days to be classified as fast ice (Fraser et al., 2010), but still had a significant amount of time-consuming and intensive manual analysis. Considerable progress has since been made in the automated extraction of the fast-ice edge in both MODIS (Fraser et al., 2019) and SAR image products (e.g., Kim et al., 2020; Li et al., 2018), in parallel with advancements in SAR-based fast ice detection in the Arctic e.g., Mahoney et al. (2007), Meyer et al. (2011) and

https://doi.org/10.5194/essd-2020-99
Preprint. Discussion started: 15 June 2020

Dammann et al. (2019). Improved automation is particularly important given the volume of data involved and the considerable effort that is required to manually digitize the fast ice edge using non-automated techniques (Fraser et al., 2012).

To date, large-scale and long time-series mapping of Antarctic fast ice has been confined to two datasets. These are: (1) the manually-classified MODIS-based dataset (Fraser et al., 2012); and (2) a fully automated Advanced Microwave Scanning Radiometer for EOS (AMSR-E)-derived time series for the time period 2003 to 2012 from Nihashi and Ohshima (2015). While the latter dataset is circumpolar in its coverage, an analysis by Fraser et al. (2019) shows a tendency of passive-microwave radiometry to underestimate fast-ice extent due to an inherent insensitivity to young fast ice $<$90 days old, and its relatively poor spatial resolution.

Here, we introduce and provide details of a new gap-filling algorithm and dataset - the first high spatio-temporal resolution (1 km; 15-day) long-term time series (currently 2000 to 2018 with regular updates planned) of complete circum-Antarctic fast ice extent. This is based on the compositing of MODIS cloud-free visible and TIR images using a technique described by Fraser et al. (2009), but improved and with automated extraction (as far as possible) of the fast ice edge through addition of edge-detection logic. This reduces the amount of manual interpretation required while increasing the level of objectivity in retrieving the fast ice maps. Importantly from both science and logistical perspectives, this ground-breaking new dataset enables improved analysis of trends and variability in the coastal Antarctic sea ice environment - to address the major knowledge gap in IPCC reports (Vaughan et al., 2013; Meredith et al., 2019). It also has a multitude of potential scientific and operational uses, given the wide-ranging importance of fast ice. Moreover, the new algorithm developed will provide an important means of mapping and monitoring fast ice into the future and in a continuous fashion, given its applicability to the new generation of medium-resolution spectroradiometers. These include the Visible Infrared Imaging Radiometer Suite (VIIRS) on NASA's Suomi National Polar-orbiting Partnership (NPP) platform (launched October 2011); the Sea and Land Surface Temperature Radiometer (SLSTR) and Ocean and Land Colour Instrument (OLCI) on ESA's Sentinel-3 platform (launched February 2016); and the Second-generation Global Imager (SGLI) on JAXA's Global Change Observation Mission (GCOM)-C1 platform (launched December 2017).

In the next sections, we present a description of the datasets and updated methods used to transform MODIS imagery into consistent fast ice maps. Following this, we present the fast ice dataset and provide a comparison with the earlier East Antarctic fast ice time series from Fraser et al. (2012). Analysis of the time series, anomalies and trends for the entire circumpolar record is beyond the scope of this paper, and is the subject of another study (Fraser et al., in prep.). A major aim here is to make this dataset available to the wider scientific community, thereby facilitating collaborative fast ice-related research across disciplines.

https://doi.org/10.5194/essd-2020-99
Preprint. Discussion started: 15 June 2020

Table 1. Table detailing techniques used to detect and/or map Antarctic fast ice, encompassing both large-scale and case studies. MODIS: Moderate Resolution Imaging Spectroradiometer (NASA). AVHRR: Advanced Very High Resolution Radiometer (NOAA). SAR: Synthetic Aperture Radar. SSM/I: Special Sensor Microwave/Imager (Defence Meteorological Satellite Program). AMSR-E: Advanced Microwave Scanning Radiometer for Earth Observation System (Japan Aerospace Exploration Agency). AMSR-2: Advanced Microwave Scanning Radiometer-2 (Japan Aerospace Exploration Agency). ALOS: Advanced Land Observing Satellite (Japan Aerospace Exploration Agency). PALSAR: Phased Array type L-band Synthetic Aperture Radar (onboard ALOS). Envisat: Environment Satellite (European Space Agency). ASAR: Advanced Synthetic Aperture Radar (onboard Envisat). RADARSAT: Radar Satellite (Canadian Space Agency).

Product	Large scale dataset or case study?	Instrument	Technique	Timespan	Temporal resolution	Spatial resolution	Spatial coverage	Advantages	Disadvantages	Publications
This work	Large scale dataset; ongoing	MODIS visible/ thermal IR	Semi-automated, composite-based	Mar 2000 – Mar 2018; updates planned	15 day	1 km	Circum-Antarctic	High spatio-temporal resolution; close agreement with Fraser et al. (2012); long and continuous time series; semi-automated	A degree of subjectivity remains; considerable manual overhead	This work
MODIS manually-digitised dataset	Large scale dataset; discontinued	MODIS visible/ thermal IR	Fully manual, composite-based	Mar 2000 – Dec 2008	20 day	2 km	East Antarctica	Medium spatio-temporal resolution; continuous time series	Fully manual	Fraser et al. (2009, 2010, 2012)
Ad-hoc MODIS and AVHRR digitisations	Case studies	MODIS and AVHRR visible/ thermal IR	Fully manual, snapshots	Nov 1978 – present	Snapshots	1 to 4 km	Focus regions	Long time series	Poor georeferencing and resolution at times (AVHRR), cloud-affected, fully manual, snapshots	Massom et al. (2009); Massom (2003); Labrousse et al. (2019); Kim et al. (2018); Aoki (2017); Ushio (2006); Mae et al. (1987)
National Ice Center charts	Large scale dataset; ongoing	Various sources (SAR, visible, TIR, scatterometer)	Fully manual, snapshots	Jul 1998 – present	Snapshots within one week	Data- and year-dependent	Circum-Antarctic	Long time series; near-real time	Unvalidated; fast ice retrieval of variable accuracy; not a consistent circumpolar product; format changes; many analysts; fully manual; coarse spatial resolution at times	N/A
Passive microwave spectral	Large scale dataset; ongoing	SSM/I, AMSR-E, AMSR-2	Principal component analysis	Dec 1990 – present	90 day	6.25 to 12.5 km	Circum-Antarctic	Fully automated	Insensitive to young (<90 day old) fast ice; coarse spatial resolution	Tamura et al. (2007, 2016); Nihashi and Ohshima (2015)
Object-based SAR	Case study	ALOS PALSAR	Object-based definition	Snapshots in 2007 and 2010	5 day	100 m	Various west Antarctic sites	Very high spatial resolution; reasonable accuracy; potential for extensive automation	Limited time series of underlying data	Kim et al. (2020)
SAR gradient difference	Case study	Envisat ASAR, Sentinel-1	Automated ice edge from gradient difference	Snapshots in 2008 and 2016	13 to 20 day	40 m	Prydz Bay	Very high spatial resolution; high accuracy; potential for extensive automation	Requires reference fast ice climatology to remove spurious edges; limited time series of underlying data	Li et al. (2018)
Motion-based SAR	Case Study	RADARSAT	Maximum cross-correlation	Snapshots in 1997 and 1999	1 to 20 day	100 m	Western Pacific Ocean sector	Very high spatial resolution; potential for extensive automation	Limited time series of underlying data	Giles et al. (2008)
Multisensor fusion	Large scale dataset; discontinued	MODIS, AMSR-E, SSM/I	Machine learning	2003 to 2008	20 day	25 km	Circum-Antarctic	Novel technique; automated	Low spatial resolution; apparent fast ice overestimate	Kim et al. (2015)

https://doi.org/10.5194/essd-2020-99
Preprint. Discussion started: 15 June 2020

Open Access Earth System Science Data Discussions

2 Dataset and methods

The new fast ice time series for the entire Antarctic coastline uses imagery (dating back to 2000) from NASA's MODIS sensors on both the Terra (MOD) and Aqua (MYD) satellites, and obtained from NASA's Level-1 Atmosphere Archive & Distribution System Distributed Active Archive Center (https://ladsweb.modaps.eosdis.nasa.gov). The first ∼2 years of this dataset was produced using only Terra MODIS imagery, prior to the July 2002 commissioning of Aqua MODIS. Specifically, the algorithm uses data from the following:

- Channel 1 (visible, 620 to 670 nm) from the MOD/MYD02QKM dataset, the 250 m resolution level 1B product being available during times of solar illumination;
- Channel 31 (thermal infrared, 10.78 to 11.28 μm) from MOD/MYD021KM, the 1 km resolution level 1B product being available regardless of sunlight and providing information during periods of polar darkness;
- The high resolution georeferencing arrays from the MOD/MYD03 product; and
- The level 2 cloud mask product (MOD/MYD35_L2).

A crucial feature of the new algorithm and time series is accurate masking of the Antarctic continent, ice shelves and nearshore islands. For this, we use the MODIS-based Mosaic Of Antarctica (MOA) coastline digitisation – both the 2003-04 product (Haran et al., 2005; Scambos et al., 2007) and the 2008-09 product (Haran et al., 2014). Change in ice-shelf front location over time due to ice-sheet advance or iceberg calving necessitates progressive updates to the MOA coastline product. For this, we make annual modifications to the location of the ice-sheet margin (coastline) by manually digitising (change in) the position of the ice shelf front in successive 15-day visible composite images at the time of annual climatological minimum fast ice extent i.e., day of year 061-075 (Fraser et al., 2012). Temporal compositing is required, and carried out, to create cloud-free images of the Antarctic coastal zone. The MOA-derived annual coastline rasters are also manually edited to correct an artefact in the coastline in the Vestfold Hills region, near Davis Station (68.5° S, 78.25° E).

All swath-to-grid projection of the level 1 and 2 imagery is performed with the MODIS Swath-To-Grid Toolkit (MS2GT, version 0.26), available at https://nsidc.org/data/modis/ms2gt. We grid all level 1 and 2 products to a 1 km resolution polar stereographic grid with a latitude of true scale set to 70° S (grid size: 5625 * 4700 pixels, covering the expected maximum circumpolar fast ice extent), to maximise compatibility with other sea ice datasets from the NSIDC. All data are provided as Climate and Forecast (CF)-compliant NetCDF files.

We broadly follow the fast ice mapping methodology developed by Fraser et al. (2009) and Fraser et al. (2010), but with significant improvements to enhance automation and objectivity in delineation of the fast ice edge. The earlier work (which focused on East Antarctica only) first constructed cloud-free composite images of the surface over consecutive 20 day periods, based on MODIS visible and TIR imagery and the NASA MODIS cloud mask product. These composites were then used for manual delineation of the fast ice edge (Fraser et al., 2010). The authors noted regions and times of lower composite image quality when persistent cloud obscured the surface in the majority of component images (cloud is a major issue for optical

https://doi.org/10.5194/essd-2020-99
Preprint. Discussion started: 15 June 2020

remote sensing of the surface in polar regions). In the Fraser et al. (2009) algorithm, even an optically-thin layer of cloud in which the surface features were still discernible was excluded from the cloud-free composite image, sometimes resulting in "data holes" in the image time series. Here, we mitigate this shortcoming by: 1) increasing the number of images contributing to the composite (thereby increasing the chance of a cloud-free view of the surface); and 2) implementing automated determination of the fast ice edge location in an independent image processing pathway which does not rely on the cloud mask product. In this latter processing pathway, we perform edge detection on all individual gridded MOD/MYD02 granules (exploiting the difference in both albedo and infrared brightness temperature between ice, cloud and ocean). This is based on the fact that both cloud and pack ice edges are dynamic between images whereas fast ice edges are likely to be relatively persistent in location (i.e., stationary). We use the Canny edge detection method (Canny, 1986) to ensure that edges are correctly localised and detected only once. We then sum all edges within a 15-day window, thereby determining which edges are (most) persistent. These persistent edges are then interpreted to be either the fast ice edge or the continental margin. Since the locations of continental margin change are well-known (on much longer time-scales), we exclude these edges from consideration and are thus left with a representation of the fast ice edge. This map of persistent edges over each 15-day window forms the basis for subsequent automated circum-Antarctic fast ice edge detection. An advantage of this approach is that it is less affected by thin cloud compared to the earlier image preparation techniques in Fraser et al. (2009), leading to a more complete time series.

Our image processing pipeline is outlined below. For each 15-day window in the March 2000 to March 2018 study period, we:

1. Download and grid all MOD/MYD35_L2 (cloud mask) granules covering the Antarctic coastal zone (approximately 1,800 granules per 15-day interval).

2. Rank granules by cloud content.

3. Select the top 600 cloud-free granules, cognizant of granule location (to ensure sufficient coverage in all coastal regions).

4. Download and grid all corresponding MOD/MYD02QKM (available during periods of solar illumination), MOD/MYD021KM and MOD/MYD03 granules.

5. Process gridded MOD/MYD02 images for manual and automated edge-detection purposes:

   – Produce cloud-free composite images: Construct thermal infrared and (when solar illumination available) visible cloud-free composite images from the gridded MOD/MYD02 and MOD/MYD35_L2 granules, following Fraser et al. (2009) and Fraser et al. (2010).

   – Produce Canny edge images: Canny edge-detect MOD/MYD02 granules and sum over successive 15-day periods.

   – Produce Sobel edge images (Sobel, 2014): Sobel edge-detect MOD/MYD02 granules and sum over successive 15-day periods (for use with manual edge delineation).

   – Produce gradient-median-composite images: Median-filter (7*7 pixel window) cloud-free composite images and calculate the absolute value of the gradient of this image, indicating edges in the composite image.

https://doi.org/10.5194/essd-2020-99
Preprint. Discussion started: 15 June 2020

- Produce modified lead-detection images after Willmes and Heinemann (2015), but with a larger filtering window of 251 pixels (originally 51 pixels) to enhance contrast in regions of fast ice.

6. Construct an automated classification base image:

   - Compute the per-pixel product of the Canny edge image and the gradient-median-composite image described above. This product represents a continuous measure of fast ice edge confidence.
   - Produce a normalised histogram of edge confidence, setting four adaptive thresholds are set at 0.995 (highest-confidence edge), 0.990, 0.985 and 0.980 (lowest-confidence edge).
   - Mask an edge confidence map by rasterised MOA coastline and write out as the automated classification base image. Multiple spurious edges exist at this point.

7. Carry out necessary manual processing:

   - Close inspection of automated classification base image, guided by: a) the Sobel edge image; b) cloud-free composites; and c) modified lead-detection images. This is used to: i) verify automated fast ice edge extraction, and ii) manually complete/add edges where automated extraction fails to detect the fast ice edge. Sobel edge detection is used in this step, rather than Canny edge detection, because it produces a broader (i.e., several pixels wide) edge which is tolerant of small changes in ice edge location.
   - “Bucket fill” those pixels between the continental margin and the (now-continuous) ice edge to represent fast ice coverage (extent).

8. Automatically remove spurious edges (i.e., edges not adjacent to fast ice) remaining from the base image.

Both the cloud-free composite images and the automated classification base images are susceptible to a number of factors which can reduce their quality/utility as fast ice edge discriminators. These include: 1) persistent/heavy cloud obscuration of the surface; and 2) instances where moving pack ice is advected toward the fast ice edge, thereby reducing the fast ice-pack ice contrast in both visible and TIR images, as noted in Fraser et al. (2009). Since the final “bucket fill” step requires a continuous fast ice edge, and because the automatically-determined fast ice edge is often incomplete, manual intervention is frequently required both to form a continuous fast ice edge and to validate the position of the automatically-determined fast ice edge. An example classification showing both manual and automated ice edge detection is shown in Figure 1. This manual intervention is time-consuming and reduces objectivity to some extent, but is considered to be a fundamental step in visible/TIR fast ice extent retrieval. It should be reiterated here that the inclusion of automatic edge determination is a considerable advance from the original fully-manual final step of edge extraction described by Fraser et al. (2010). In order to mitigate the possibility of manual edge definition contributing to false trends in the dataset and following Fraser et al. (2012), all edge verification and manual edge completion is performed in a random order.

When manual edge delineation is not possible in any given region for a particular 15-day period (e.g., due to persistent thick cloud), the method employs a subjective definition of the location of the fast ice edge based on imagery from the immediately

https://doi.org/10.5194/essd-2020-99
Preprint. Discussion started: 15 June 2020

previous and/or subsequent 15-day periods, following Fraser et al. (2010). An extreme example relates to the fast ice map from DOY 166-180 in 2001, during most of which the Terra MODIS instrument was in "safe mode" and acquired no data. Here and in the interest of providing a temporally-contiguous dataset, we opt to use the fast ice map from the following timestep (DOY 181-195, 2001) but mark all edges as "manually-determined" to indicate higher uncertainty in the fast ice edge retrieval for DOY 181-195 (2001).

Determination of uncertainty for this dataset (in both edge location and resulting fast ice areal extent) requires careful consideration. The primary uncertainty arises from digitisation error (typically given in pixels) in areas of manual ice edge determination, which then propagates to an areal uncertainty value. However, neither the digitisation error nor the propagation to an areal uncertainty are straightforward to determine/quantify. Prior work made broad estimates of the manual digitisation error by carrying out an independent re-digitisation of a subset of the fast ice edge and resolving differences in the resulting fast ice area (Fraser et al., 2010). This approach, however, requires both extrapolation of errors from a small subset to the entire dataset and duplication of time-consuming manual edge extraction. In our modified approach (presented here), we employ a novel alternative approach for uncertainty estimation which addresses these shortcomings. This involves analysis of the per-pixel difference in ice edge location in two consecutive fast ice maps, for all pairs of consecutive images in the entire dataset. In the case of an automatically-extracted fast-ice edge pixel, this difference purely reflects the change in location of the ice edge. In the case of a manually-extracted ice edge pixel, it reflects the sum of the ice edge change plus the digitisation error. Thus, to estimate the digitisation uncertainty, we:

1. assume that automatically-determined edges are accurate in location (an appropriate assumption due to excellent edge localisation of the Canny edge detection filter underpinning the automation);

2. quantify the mean fast ice edge separation between subsequent images only for automatically-determined edge pixels, to produce a mean measure of ice edge location change between two consecutive 15-day time periods;

3. quantify the mean fast ice edge separation between subsequent images only for manually-determined edge pixels, to produce a mean measure of ice edge change plus digitisation error; and

4. subtract the former from the latter, resulting in a digitisation error estimate for manually-determined ice edge pixels.

Following estimation of the manual digitisation error, we estimate areal uncertainty for each fast ice map by: 1) ensuring that the manually-determined fast ice edge is one pixel wide by performing a morphological skeleton operation; 2) weighting all remaining manually-determined pixels by their respective area; then 3) multiplying by the digitisation error, as estimated above. This approach to areal uncertainty calculation is highly conservative (i.e., likely an overestimate) since it assumes that all errors occur in the same direction; in reality, digitisation errors are likely to produce both underestimates and overestimates of fast ice extent in equal measure. Furthermore, cyclonic systems which may cause wind-blown regional fast ice breakout (Massom et al., 2009) also typically bring extensive cloud cover. In this way, image subsets requiring manual fast ice edge delineation are more likely to be produced during times of wholesale ice edge change, thereby falsely inflating the uncertainty estimates.

https://doi.org/10.5194/essd-2020-99
Preprint. Discussion started: 15 June 2020

Regarding the fast ice dataset product, we provide the method of edge determination ("automatic" or "manual") in the output dataset, for each pixel of fast ice edge. We also compute the mean percentage of automatically-determined ice edge pixels in each 1° longitude bin. As a further indication of dataset integrity, we quantify differences between the new fast ice dataset and the Fraser et al. (2012) East Antarctic-only dataset for the period and region of overlap (10° W to 172° E, north of 72° S, March 2000 to December 2008). Large tabular icebergs are removed from the fast ice classification where independent iceberg information is available and/or the icebergs are clearly visible, but manual discrimination between fast ice and large tabular icebergs is difficult at times due to a lack of contrast in the satellite imagery(Fraser et al., 2010). Similarly, myriads of small icebergs embedded/grounded in places in the fast ice (Massom et al., 2009) are difficult to distinguish and remove, but form an integral part of the fast ice matrix. Following Fraser et al. (2010), we classify such regions of fast ice containing many small grounded icebergs as fast ice.

3 Results and brief discussion

Here, we restrict our presentation of results to illustrating the key attributes of this ground-breaking new dataset in its circumpolar entirety, while also evaluating improvements compared to the earlier mapping of fast-ice extent (across East Antarctica) by Fraser et al. (2012) and uncertainties. More in-depth analysis of spatial-temporal patterns of fast ice distribution (based on this dataset), and their drivers, is outside the scope of this journal but is underway (Fraser et al., in prep.).

3.1 Circumpolar distribution of fast ice at maximum and minimum extent, and cross-comparison with earlier work

We illustrate the envelope of circum-Antarctic fast ice extent throughout the 18-year dataset time series by showing its spatial distribution at maximum (occurring in 2006, at DOY 271-285) and minimum (2009, DOY 061-075) extent in Figure 2. Figure 3 then shows a cross-comparison of this important new dataset with that of Fraser et al. (2012), covering the area and period of overlap. The total East Antarctic fast ice extent in the new dataset is 8.3 % greater than that reported in Fraser et al. (2012), on average. This difference is attributed to two factors: 1) a "relaxation" of the temporal fast ice condition in the new algorithm (from the 20-day criterion used in Fraser et al. (2012), i.e., more ice remains "fast" (stationary) for 15 days than for 20 days); and 2) the enhanced ability of the new "persistence of edges" algorithm to retrieve fast-ice extent under cloud cover. The largest differences between the two datasets are encountered at ∼118° E and 152° E. These two longitudes correspond to areas of dynamically-formed "semi-fast ice", i.e., regions where pack ice is blocked from westward advection (and intercepted) by upstream obstacles e.g., large grounded iceberg B9B prior to its ungrounding in 2010 (Massom et al., 2010). In such regions, fast ice tends to be more exposed and ephemeral i.e., it can intermittently break out to become pack ice but then reform, on a synoptic scale. As such, reducing the temporal "fastness" condition (to 15 days) produces relatively large differences in these regions.

https://doi.org/10.5194/essd-2020-99
Preprint. Discussion started: 15 June 2020

3.2 Quantification of dataset objectivity and error estimation

A broad measure of objectivity in fast ice extent retrieval is the percentage of edges that could be retrieved automatically. This is plotted in Figure 4. The circum-Antarctic mean automation percentage is 58%. East Antarctica is characterised by generally high automation percentages (∼50 to 90%) – with the exception of localised pockets (down to 37%) located in Wilkes (98° to 108° E and 126° to 138° E) and George V lands (150° to 153° E). In West Antarctica, automation percentage is high (generally 70 to 90%) in the eastern Weddell Sea and Ross Sea (50 to 85%), but low in the Bellingshausen and Amundsen seas sector (40 to 60%) and along both flanks of the Antarctic Peninsula (as low as 22%). This plot also indicates areas which tend to be most affected by inherent issues detailed in the Methods Section, i.e., persistent cloud cover and/or persistent advection of pack ice toward fast ice that reduces the contrast in (reflectance and surface temperature) between pack and fast ice.

As detailed in the Methods Section, we developed a novel technique to quantify the error in manual estimation of fast ice edges. We find that, on average, manually-determined edges temporally vary in location by 5.47 pixels more than automatically-determined edges (auto-determined = 10.06 pixels vs manually-determined = 15.53 pixels). For each 15-day epoch, we obtain a conservative estimate of the fast ice areal uncertainty by multiplying the number of manually-determined pixels by the equivalent distance of 5.47 km, assuming that the nominal resolution of 1 km/pixel applies everywhere in the domain. This uncertainty in fast-ice area has a mean value of 7.3 % when averaged across the entire circum-Antarctic dataset. This is similar to the value of 4.38% uncertainty obtained in regions requiring >10% manual edge delineation, as detailed in Figure 5 from Fraser et al. (2010) using traditional re-digitisation-based error estimation, confirming that the new method is conservative.

4 Summary

Here we have both introduced: 1) a new improved technique for mapping and monitoring coastal fast ice coverage around Antarctica at high resolution, and 2) the most complete time series of Antarctic fast ice extent to date. This ground-breaking product represents an important new baseline against which to gauge change and variability in both the ice and climate, and has wide applicability. Indeed, it is expected to generate and contribute to multiple cross-disciplinary studies of the Antarctic coastal environment. Moreover, it directly addresses a key gap identified in major high-level IPCC reports regarding the highly-vulnerable Antarctic coastal environment (Vaughan et al., 2013; Meredith et al., 2019).

Although an element of subjectivity remains in the large-scale retrieval of fast ice coverage from satellite visible/thermal infrared imagery, we have mitigated this to some extent. This has been achieved by: a) implementing an automated ice edge-retrieval algorithm (resulting in successful extraction of ∼58% of ice edge pixels); b) performing random manual extraction to eliminate false trends; c) quantifying the uncertainty associated with manual edge delineation (7.3 % of fast ice area retrieval, on average); and d) performing a cross-comparison with a similar (but independent)spatially- and temporally-overlapping dataset (Fraser et al., 2012). Crucially, this new MODIS-based dataset provides the longest contiguous time series of this key element of the Antarctic cryosphere while offering complete circum-Antarctic coverage for the first time at high resolution.

Analysis of spatio-temporal patterns, variability and trends in circum-Antarctic fast ice coverage is underway, using this dataset (Fraser et al., in prep.), as is related work determining and evaluating the drivers of these observed patterns. Moreover,

https://doi.org/10.5194/essd-2020-99
Preprint. Discussion started: 15 June 2020

we plan to study the spatial distribution of fast ice extent in the context of a major new coastal configuration and complexity dataset for Antarctica (Porter-Smith et al., in review, 2019), to explore possible linkages.

5 Data availability

The dataset has been made available at the Australian Antarctic Data Centre at http://dx.doi.org/doi:10.26179/5d267d1ceb60c, as a series of NetCDF files (Fraser et al., 2020). This dataset contains the following fields:

- Fast ice time series - presented as classified maps of the surface type (fast ice interior pixel; automatically-determined fast ice edge; manually-determined fast ice edge); and
- Latitude, longitude and area of each pixel.

There are plans to regularly update and extend the time series forwards in time, on a biennial basis, until the demise of both MODIS platforms but continuing with next-generation imaging spectroradiometers after this time.

Author contributions. ADF led the study, acquired the data, developed automation algorithms, manually digitised fast ice, produced figures, and wrote the manuscript. RAM and KIO contributed equally toward project genesis and direction. SW contributed to algorithm automation development. PJK assisted with manual digitisation. JC and RP-S packaged the dataset for distribution. All authors edited the manuscript.

Competing interests. The authors declare that they have no conflict of interest.

Acknowledgements. MODIS data were obtained from the NASA Level-1 Atmosphere Archive & Distribution System Distributed Active Archive Center at: https://ladsweb.modaps.eosdis.nasa.gov. This work was supported by the Australian Government's Cooperative Research Centre program through the Antarctic Climate & Ecosystems Cooperative Research Centre; the Japan Society for the Promotion of Science Grant-in-Aid for Scientific Research (KAKENHI) numbers 25·03748, 24·810030, 25·241001 and 26·740007; by the Canon Foundation; the Natural Environment Research Council (Grant NE/L002531/1); and the Australian Research Council's Special Research Initiative for Antarctic Gateway Partnership (Project ID SR140300001). This work also contributes to Australian Antarctic Science Project 4116, the Australian Antarctic Program Partnership and the World Climate Research Programme (WCRP) Climate and Cryosphere (CliC) Project initiative *Interactions Between Cryospheric Elements*. RM acknowledges the support of the Australian Antarctic Division. ADF is grateful to D. Fanning for maintaining the Coyote library of IDL routines, many of which were used in this work, to T. Haran (NSIDC) for developing the MODIS Swath-To-Grid Toolbox, and to C. Greene for discussions around the distribution of the data.

References

Aoki, S.: Breakup of landfast sea ice in Lützow-Holm Bay, East Antarctica, and its teleconnection to tropical Pacific sea surface temperatures, Geophysical Research Letters, 44, 3219 – 3227, 2017.

Canny, J.: A Computational Approach to Edge Detection, IEEE Transactions on Pattern Analysis and Machine Intelligence, 6, 679 – 698, 1986.

Dammann, D. O., Eriksson, L. E. B., Mahoney, A. R., Eicken, H., and Meyer, F. J.: Mapping pan-Arctic landfast sea ice stability using Sentinel-1 interferometry, The Cryosphere, 13, 557–577, https://doi.org/10.5194/tc-13-557-2019, https://www.the-cryosphere.net/13/557/2019/, 2019.

Fraser, A. D., Massom, R. A., and Michael, K. J.: A Method for Compositing Polar MODIS Satellite Images to Remove Cloud Cover for Landfast Sea-Ice Detection, IEEE Transactions on Geoscience and Remote Sensing, 47, 3272–3282, https://doi.org/10.1109/TGRS.2009.2019726, 2009.

Fraser, A. D., Massom, R. A., and Michael, K. J.: Generation of high-resolution East Antarctic landfast sea-ice maps from cloud-free MODIS satellite composite imagery, Remote Sensing of Environment, 114, 2888–2896, https://doi.org/10.1016/j.rse.2010.07.006, 2010.

Fraser, A. D., Massom, R. A., Michael, K. J., Galton-Fenzi, B. K., and Lieser, J. L.: East Antarctic Landfast Sea Ice Distribution and Variability, 2000-08, Journal of Climate, 25, 1137–1156, https://doi.org/10.1175/JCLI-D-10-05032.1, 2012.

Fraser, A. D., Ohshima, K. I., Nihashi, S., Massom, R. A., Tamura, T., Nakata, K., Williams, G. D., Carpentier, S., and Willmes, S.: Landfast ice controls on sea-ice production in the Cape Darnley Polynya: A case study, Remote Sensing of Environment, 233, https://doi.org/https://doi.org/10.1016/j.rse.2019.111315, 2019.

Fraser, A. D., Massom, R. A., Ohshima, K. I., Willmes, S., Kappes, P., Cartwright, J., and Porter-Smith, R.: Circum-Antarctic landfast sea-ice extent, 2000-2018, Online dataset, http://dx.doi.org/doi:10.26179/5d267d1ceb60c, 2020.

Giles, A. B., Massom, R. A., and Lytle, V. I.: Fast-ice distribution in East Antarctica during 1997 and 1999 determined using RADARSAT data, Journal of Geophysical Research (Oceans), 113, https://doi.org/10.1029/2007JC004139, 2008.

Haran, T. M., Bohlander, J., Scambos, T. A. Painter, T., and Fahnestock, M. A.: MODIS Mosaic of Antarctica 2003-2004 (MOA2004) image map, Digital media, http://dx.doi.org/10.7265/N5ZK5DM5, 2005.

Haran, T. M., Bohlander, J., Scambos, T. A., Painter, T., and Fahnestock, M. A.: MODIS Mosaic of Antarctica 2008-2009 (MOA2009) image map, Digital media, http://dx.doi.org/10.7265/N5KP8037, 2014.

Kim, M., Im, J., Han, H., Kim, J., Lee, S., Shin, M., and Kim, H.-C.: Landfast sea ice monitoring using multisensor fusion in the Antarctic, GIScience & Remote Sensing, 52, 239 – 256, 2015.

Kim, M., Han, H., Im, J., Lee, S., and Kim, H.-C.: Object-based Landfast Sea Ice Detection Over West Antarctica Using Time Series of ALOS PALSAR Data, Remote Sensing of Environment, 242, 2020.

Kim, S., Saenz, B., Scanniello, J., Daly, K., and Ainley, D.: Local climatology of fast ice in McMurdo Sound, Antarctica, Antarctic Science, 30, 125–142, https://doi.org/10.1017/S0954102017000578, 2018.

Labrousse, S., Fraser, A. D., Sumner, M., Tamura, T., Pinaud, D., Wienecke, B., Kirkwood, R., Ropert-Coudert, Y., Reisinger, R., Jonsen, I., Porter-Smith, R., Barbraud, C., Bost, C.-A., Ji, R., and Jenouvrier, S.: Dynamic fine-scale sea-icescape shapes adult emperor penguin foraging habitat in East Antarctica, Geophysical Research Letters, 46, 11 206 – 11 218, 2019.

https://doi.org/10.5194/essd-2020-99
Preprint. Discussion started: 15 June 2020

Li, X., Ouyang, L., Hui, F., Cheng, X., Shokr, M., and Heil, P.: An Improved Automated Method to Detect Landfast Ice Edge off Zhongshan Station Using SAR Imagery, IEEE Journal of Selected Topics in Applied Earth Observations and Remote Sensing, 11, 4737–4746, https://doi.org/10.1109/JSTARS.2018.2882602, 2018.

Lubin, D. and Massom, R. A.: Polar Remote Sensing Volume I: Atmosphere and Oceans, Praxis/Springer, Chichester/Berlin, 2006.

Mae, S., Yamanouchi, T., and Fujii, Y.: Remote sensing of fast ice in Lützowholmbukta, East Antarctica, using satellite NOAA-7, 8 and aircraft, Annals of Glaciology, 9, 251–251, 1987.

Mahoney, A., Eicken, H., Gaylord, A. G., and Shapiro, L.: Alaska landfast sea ice: Links with bathymetry and atmospheric circulation, Journal of Geophysical Research (Oceans), 112, 2001, 2007.

Massom, R. A.: Recent iceberg calving events in the Ninnis Glacier region, East Antarctica, Antarctic Science, 15 (2), 303–313, 2003.

Massom, R. A., Hill, K., Barbraud, C., Adams, N., Ancel, A., Emmerson, L., and Pook, M.: Fast ice distribution in Adélie Land, East Antarctica: Interannual variability and implications for Emperor penguins (*Aptenodytes forsteri*), Marine Ecology Progress Series, 374, 243–257, 2009.

Massom, R. A., Giles, A. B., Fricker, H. A., Warner, R., Legrésy, B., Hyland, G., Young, N., and Fraser, A. D.: Examining the interaction between multi-year landfast sea ice and the Mertz Glacier Tongue, East Antarctica; Another factor in ice sheet stability?, Journal of Geophysical Research (Oceans), 115, C12 027, https://doi.org/10.1029/2009JC006083, 2010.

Massom, R. A., Scambos, T. A., Bennetts, L. G., Reid, P., Squire, V. A., and Stammerjohn, S. E.: Antarctic ice shelf disintegration triggered by sea ice loss and ocean swell, Nature, 558, 383 – 389, https://doi.org/https://doi.org/10.1038/s41586-018-0212-1, 2018.

Meredith, M., Sommerkorn, M., Cassotta, S., Derksen, C., Ekaykin, A., Hollowed, A., Kofinas, G., Mackintosh, A., Melbourne-Thomas, J., Muelbert, M. M. C., Ottersen, G., Pritchard, H., and Schuur, E. A. G.: IPCC Special Report on the Ocean and Cryosphere in a Changing Climate, chap. Polar Regions, p. 215, Cambridge University Press, Cambridge, 2019.

Meyer, F. J., Mahoney, A., Eicken, H., Denny, C. L., Druckenmiller, H. C., and Hendricks, S.: Mapping Arctic landfast ice extent using L-band synthetic aperture radar interferometry, Remote Sensing of Environment, 115, 3029–3043, https://doi.org/10.1016/j.rse.2011.06.006, 2011.

Nihashi, S. and Ohshima, K. I.: Circumpolar mapping of Antarctic coastal polynyas and landfast sea ice: Relationship and variability, Journal of Climate, 28, 3650–3670, 2015.

Porter-Smith, R., McKinlay, J., Fraser, A. D., and Massom, R. A.: Coastal complexity of the Antarctic continent, Earth System Science Data Discussions, https://doi.org/https://doi.org/10.5194/essd-2019-142, in review, 2019.

Scambos, T., Haran, T., Fahnestock, M., Painter, T., and Bohlander, J.: MODIS-based Mosaic of Antarctica (MOA) data sets: Continent-wide surface morphology and snow grain size, Remote Sensing of Environment, 111, 242–257, 2007.

Sobel, I.: An Isotropic 3x3 Image Gradient Operator, Presentation at Stanford A.I. Project 1968, 2014.

Tamura, T., Ohshima, K. I., Markus, T., Cavalieri, D. J., Nihashi, S., and Hirasawa, N.: Estimation of Thin Ice Thickness and Detection of Fast Ice from SSM/I Data in the Antarctic Ocean, Journal of Atmospheric and Oceanic Technology, 24, 1757–1772, https://doi.org/10.1175/JTECH2113.1, 2007.

Tamura, T., Ohshima, K. I., Fraser, A. D., and Williams, G. D.: Sea ice production variability in Antarctic coastal polynyas, Journal of Geophysical Research (Oceans), 121, 2967–2979, https://doi.org/10.1002/2015JC011537, 2016.

Ushio, S.: Factors affecting fast-ice break-up frequency in Lützow-Holm Bay, Antarctica, Annals of Glaciology, 44, 177–182, 2006.

Vaughan, D. G., Comiso, J. C., Allison, I., Carrasco, J., Kaser, G., Kwok, R., Mote, P., Murray, T., Paul, F., Ren, J., Rignot, E., Solomina, O., Steffen, K., and Zhang, T.: Climate Change 2013: The Physical Science Basis. Contribution of Working Group I to the Fifth Assess-

https://doi.org/10.5194/essd-2020-99
Preprint. Discussion started: 15 June 2020

ment Resport of the Intergovernmental Panel on Climate Change, chap. Observations: Cryosphere, p. 334, Cambridge University Press, Cambridge, 2013.

Willmes, S. and Heinemann, G.: Pan-Arctic lead detection from MODIS thermal infrared imagery, Annals of Glaciology, 56, 29–37, https://doi.org/10.3189/2015AoG69A615, 2015.

World Meteorological Organization: WMO sea-ice nomenclature. Terminology, codes and illustrated glossary, Tech. Rep. 259, Geneva Secretariat of the World Meterological Organization, 1970.

https://doi.org/10.5194/essd-2020-99
Preprint. Discussion started: 15 June 2020

Open Access Earth System Science Data Discussions

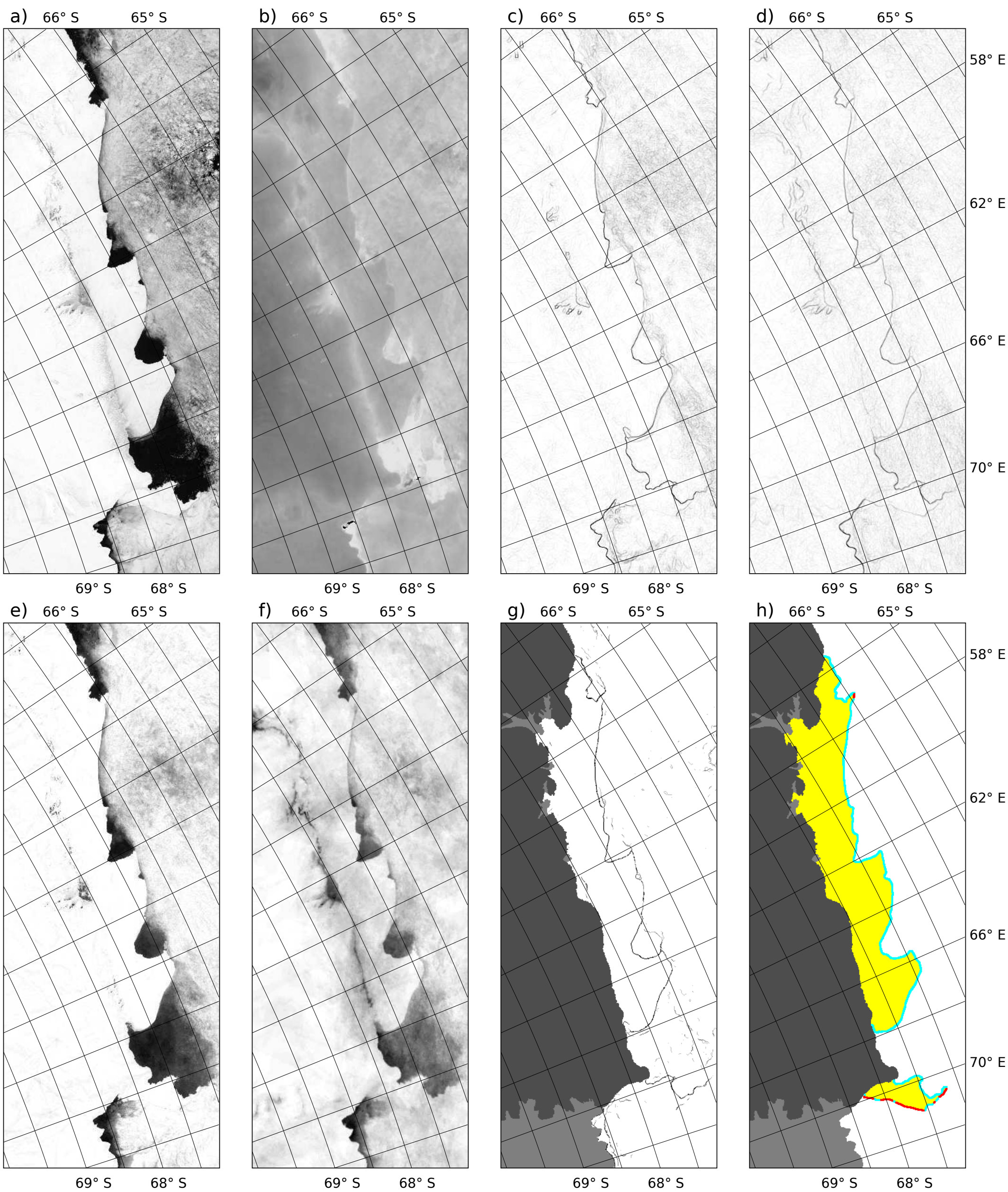

Figure 1. Figure depicting an example of the automated fast ice edge detection along the Mawson Coast, East Antarctica, for DOY range 316-330, 2005. See the red rectangle in Figure 2 for spatial context. a) and b): 15-day channel 1 (visible) and channel 31 (thermal infrared) cloud-free composite images, respectively. c) and d): Sum of Canny algorithm-detected edges in individual channel 1 and channel 31 images respectively, for the 15-day period. e) and f): Modified lead-detection for channel 1 and channel 31 images, respectively (after Willmes and Heinemann, 2015, but with an enlarged filtering window to enhance fast ice detection). g) Results of the combined edge detection algorithm (black line). Light and dark grey areas represent grounded and floating glacial ice, respectively, and are masked out. h) Fast ice classified map after manual edge inspection/correction and filling. Cyan and red represent automatically- and manually-completed edges, respectively, and the width of these lines has been expanded in this example to enhance visibility. Yellow represents infilled fast ice area.

https://doi.org/10.5194/essd-2020-99
Preprint. Discussion started: 15 June 2020

Open Access Earth System Science Data Discussions

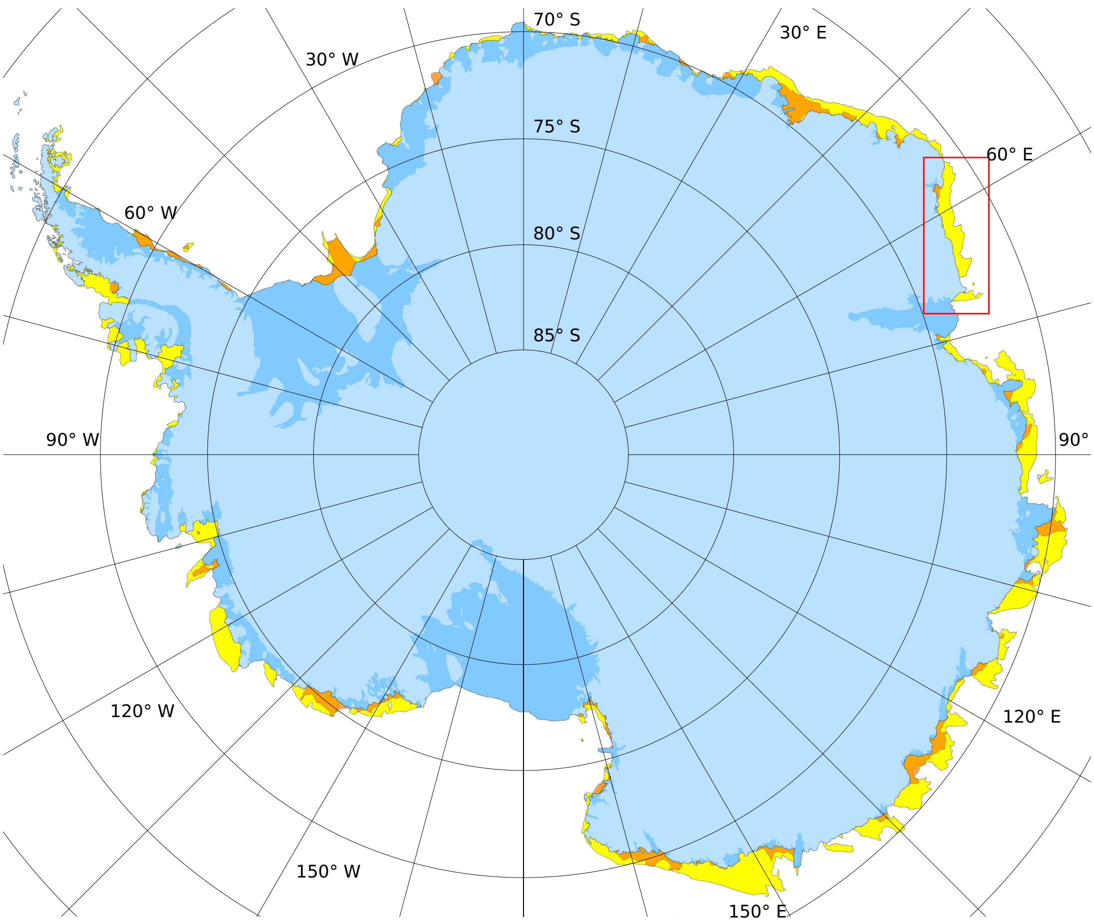

Figure 2. Fast ice distribution at times of maximum (occurring in 2006, DOY 271-285; shown in yellow) and minimum (2009, DOY 061-075; shown in orange) extent over the 18-year dataset period. The Antarctic Ice Sheet and ice shelves are shaded blue. The red rectangle shows the region used to illustrate the automation in Fig. 1

https://doi.org/10.5194/essd-2020-99
Preprint. Discussion started: 15 June 2020

Open Access Earth System Science Data Discussions

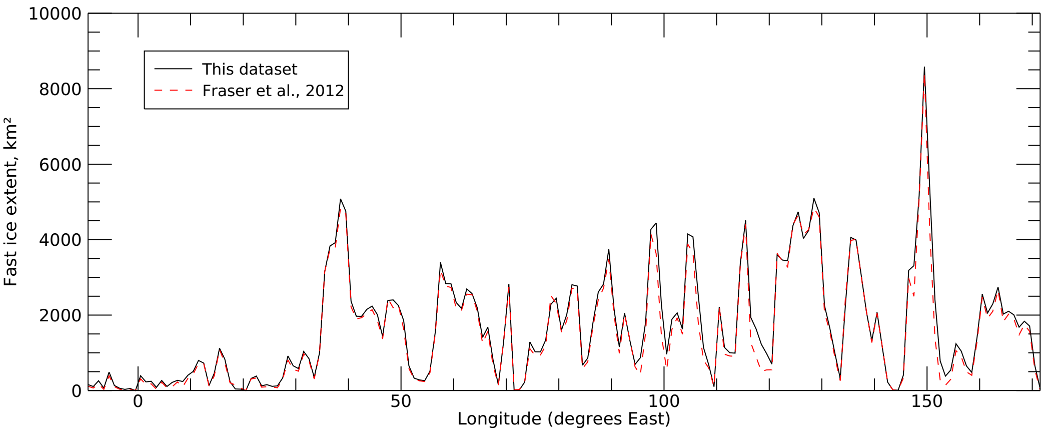

Figure 3. Mean fast ice extent per degree of longitude for this new improved dataset (black solid line) and Fraser et al. (2012) (dashed red line), for the period and region of time series overlap (March 2000 to December 2008, 10° W to 172° E).

https://doi.org/10.5194/essd-2020-99
Preprint. Discussion started: 15 June 2020

Open Access Earth System Science Data Discussions

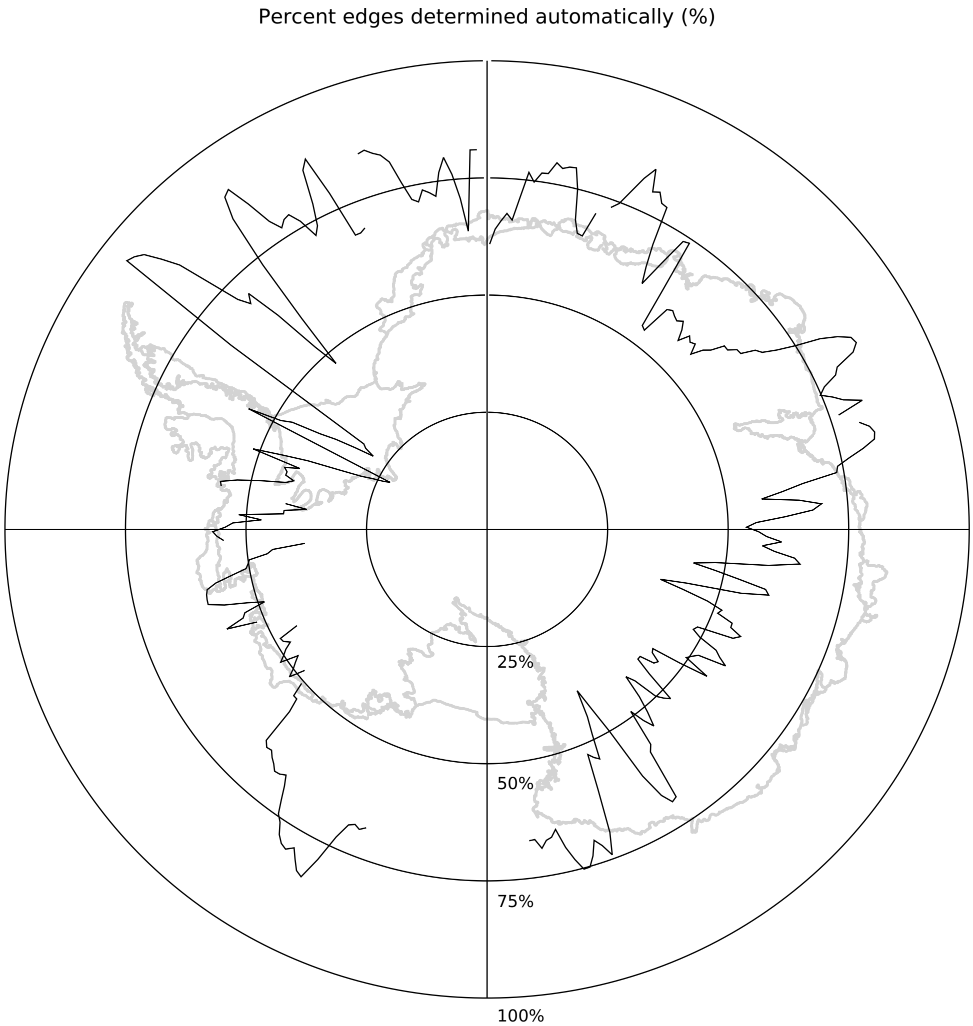

Figure 4. Polar plot showing the percentage of edges determined automatically, as a function of longitude. The Antarctic continent is outlined in grey for spatial context.